LAWRENCE
LIVERMORE
NATIONAL
LABORATORY

UCRL-JRNL-217964

Chemical Force Microscopy of Chemical and Biological Interactions

A. Noy

January 5, 2006

Surface and Interface Analysis

Disclaimer

This document was prepared as an account of work sponsored by an agency of the United States Government. Neither the United States Government nor the University of California nor any of their employees, makes any warranty, express or implied, or assumes any legal liability or responsibility for the accuracy, completeness, or usefulness of any information, apparatus, product, or process disclosed, or represents that its use would not infringe privately owned rights. Reference herein to any specific commercial product, process, or service by trade name, trademark, manufacturer, or otherwise, does not necessarily constitute or imply its endorsement, recommendation, or favoring by the United States Government or the University of California. The views and opinions of authors expressed herein do not necessarily state or reflect those of the United States Government or the University of California, and shall not be used for advertising or product endorsement purposes.

Chemical Force Microscopy of Chemical and Biological Interactions

Aleksandr Noy

Chemistry and Materials Science Directorate,
Lawrence Livermore National Laboratory,
Livermore, CA 94550, USA
E-mail: ***noy1@llnl.gov***

Abstract

Interactions between chemical functionalities define outcomes of the vast majority of important events in chemistry, biology and materials science. Chemical Force Microscopy (CFM)— a technique that uses direct chemical functionalization of AFM probes with specific functionalities — allows researchers to investigate these important interactions directly. We review the basic principles of CFM, some examples of its application, and theoretical models that provide the basis for understanding the experimental results. We also emphasize application of modern kinetic theory of non-covalent interactions strength to the analysis of CFM data.

Contents

1 Chemical Force Microscopy: Basic Setup and Measurement

1.1 Introduction

Non-covalent intermolecular interactions shape the majority of microscopic processes in chemical, biological, and artificial systems. Examples range from lock-and-key interactions that define molecular recognition, to interfacial adhesion and friction that define performance and wear of industrial equipment. Moreover, as nanotechnology begins to set the pace of modern technological advancement in areas as diverse as telecommunications and biomedical engineering, the prominence of intermolecular interactions will only increase. Potential technological and scientific payoffs from the intimate knowledge of these non-covalent bonds and the nature of their failure are enormous and could range from better drugs and medical imaging agents to wear-resistant interfaces, to super-strong and reversible adhesive joints.

Historically, non-covalent interactions have been relegated to the secondary place in chemistry, with most efforts concentrated on understanding covalent binding and chemical reactivity. Researchers studied non-covalent interactions mostly using macroscopic techniques such as calorimetry, surface tension studies, IR spectroscopy, chemical equilibrium studies, virial coefficients, and elastic moduli [1, 2, 3]. These indirect measurements have provided a wealth of the information about non-specific interactions, yet understanding the true nature of the non-covalent bonding still requires a direct measurement. A simple back-of-the-envelope estimate pegs the strength of a typical non-covalent bond to the range of the maximum gradient of a typical interaction potential, which produces estimates in the 10 pN to 1 nN interval. Variations in the surrounding medium only increase this spread. Experimental techniques that could measure forces in this range under a variety of ambient conditions and solvents have only become available during the recent decades. Specifically, three techniques are capable of such measurements: Surface Forces Apparatus (SFA) [4, 5], Optical (and Magnetic) Tweezers [6, 7], and Atomic Force Microscopy (AFM) [8, 9, 10]. Of the three techniques only AFM possesses both the sub-nanometer spatial resolution and picoNewton force resolution necessary for characterizing the strength and spatial distribution of intermolecular interactions.

AFM measurements use sharp microfabricated probes attached to the force-sensing cantilevers with spring constants ranging from 0.01 N/m to 100 N/m [11]. These probes, coupled with Angstrm-level distance measurement and positioning accuracy, give AFM the technical capabilities for measuring specific interaction forces. However, the utility of the standard AFM setup for measuring specific forces is severely limited by the unknown chemical composition of the AFM tip. Standard silicon and silicon nitride probes present a poorly defined chemical interface and often pick up contamination during the measurement. A concept of Chemical Force Microscopy, introduced by Lieber and coworkers [12], replaces poorly characterized tip-sample interface with a well-defined interface produced by deliberate functionalization of the AFM tip surface (and often the sample surface). These modifications transforms AFM from a tool for measuring ill-defined interactions of silicon probes with surfaces into a tool for measuring specific well-defined chemical interactions (Figure 1A). Careful design of the probe coating can also prevent contaminations, control the number of interacting molecules, and even separate different types of interactions spatially. Some of the progress and key results of Chemical Force Microscopy have been the subject of two detailed reviews [13, 14]. Despite their apparent simplicity, CFM measurements have already uncovered a wealth of complex behavior that even the simplest intermolecular interaction

can display during force-induced failure. This article will concentrate on exploring these behaviors and understanding them in the general context of the failure of a chemical bond under an external load.

1.2 Probe Modification and Force Measurement

Modification of the AFM probes (and often the samples) with well-defined chemical functionalities is the key to Chemical Force Microscopy. Unless a researcher wants to go through the expense of fabricating custom probes, the logical place to start is any one of the commercial microfabricated Si or Si_3N_4 probes. Although several initial attempts have used non-specific adsorption of proteins, such as BSA, to place the functionalities on the AFM tip for further chemical modification [15], the preferred current modification route goes through the creation of close-packed organic monolayers on the probe surface. For these approaches researchers typically utilize silane chemistry for direct modifications of the AFM probe surface, or pre-coat the probe surface with the thin layer of gold and subsequently form a monolayer of alkanethiols on the gold surface. Both of these approaches provide robust and well-defined coatings; the resulting monolayers can present a variety of chemical functionalities suitable for further modification. Reference [14] presents a detailed review of probe functionalization techniques.

The modification steps can produce several different arrangements of the interacting groups for CFM experiments (Figure 1). This choice can have profound implications on the nature of the interactions, as well as the type of the information available from force spectroscopy experiments. In the simplest case, all molecules at the end of the AFM tip bear the same functionality (Figure 1B). In this arrangement, the interactions between the AFM tip and the sample comprise a large number of identical specific functional group interactions. This arrangement tends to minimize the possibility of observing non-specific interactions; however, it is often impossible to estimate the exact number or the interacting functional groups. As we will show in the later sections, this arrangement generally leads to complex unbinding kinetics, with solvation effects playing a characteristically large role [16]. we also note that this type of probe tip functionalization is also common in CFM studies of polymer surfaces. The topic of CFM of polymers deserves a separate consideration due to the complex of interactions that arise during these measurements; we will not consider it here and instead point the reader to work by Vancso group [17, 18, 19].

Often researchers dilute the active functional group on the AFM tip with an inactive spacer molecule that decreases the density of the active molecules on the tip (Figure 1C).

This "dilution" approach is especially fruitful for creating systems for studying individual molecular interactions, as often researchers can adjust the dilution to limit the number of the interacting molecules to a single pair. high probability of observing non-specific interactions and, consequently, the necessity to discriminate between the relevant interactions and the non-specific background is an obvious disadvantage of this approach. As a practical consequence, researchers use this this configuration almost exclusively for studying strong distinct individual interactions, such as ligand-receptor interactions [20]. This configuration almost always requires control experiments (typically specific blocking of a surface receptor with the solution excess of one of the ligand) to prove that specific interactions have indeed been detected. Solvation still plays a role in these systems, and the unbinding kinetics often follows the rules predicted by the kinetic model for the strength of a single bond.

The third configuration involves attaching the interacting molecules to the ends of flexible polymer tethers that hang off the AFM tip (Figure 1D). The tethers play several important roles. First, they separate the non-specific interactions from the specific interactions (as in this configuration specific interactions occur only at the tip-sample separation that is equal to the combined tether length). Second, tethers allow substantial conformational freedom to the interacting molecules, that can achieve the most efficient orientation for binding. In some systems tethers can even provide a means to estimate the number of the interacting species [21], which gives researchers an important capability for studying multiple bond interactions. On the flip side, the presence of flexible tethers can lead to the situation where the measured interaction forces contain contributions from a number of possible binding orientations instead of one defined orientation.

Measuring forces with an atomic force microscope involves translating the functionalized cantilever in and out of contact with the sample surface in a so-called "force curve" cycle while recording the cantilever deflection along the way. Figure 2A and Figure 8C show several examples of the force curves. The rupture of the tip-surface bond produces a characteristic jump in the force curve, and the magnitude of that jump provides a measure of the adhesion force. Several technical aspects of the measurement are worth mentioning. First, researchers must calibrate the force constant of each cantilever used in the measurement. The actual spring constants of commercial AFM cantilevers can deviate as much as 50% from the value quoted by manufacturers; therefore individual calibration of the probes is essential. Several methods for calibrating cantilever spring constants exist [22, 23, 24], and at least one of them, fist developed by Hutter and Beechoefer [24], is increasingly becoming a standard feature of a modern atomic force microscope control software. Second, it is important to record (and

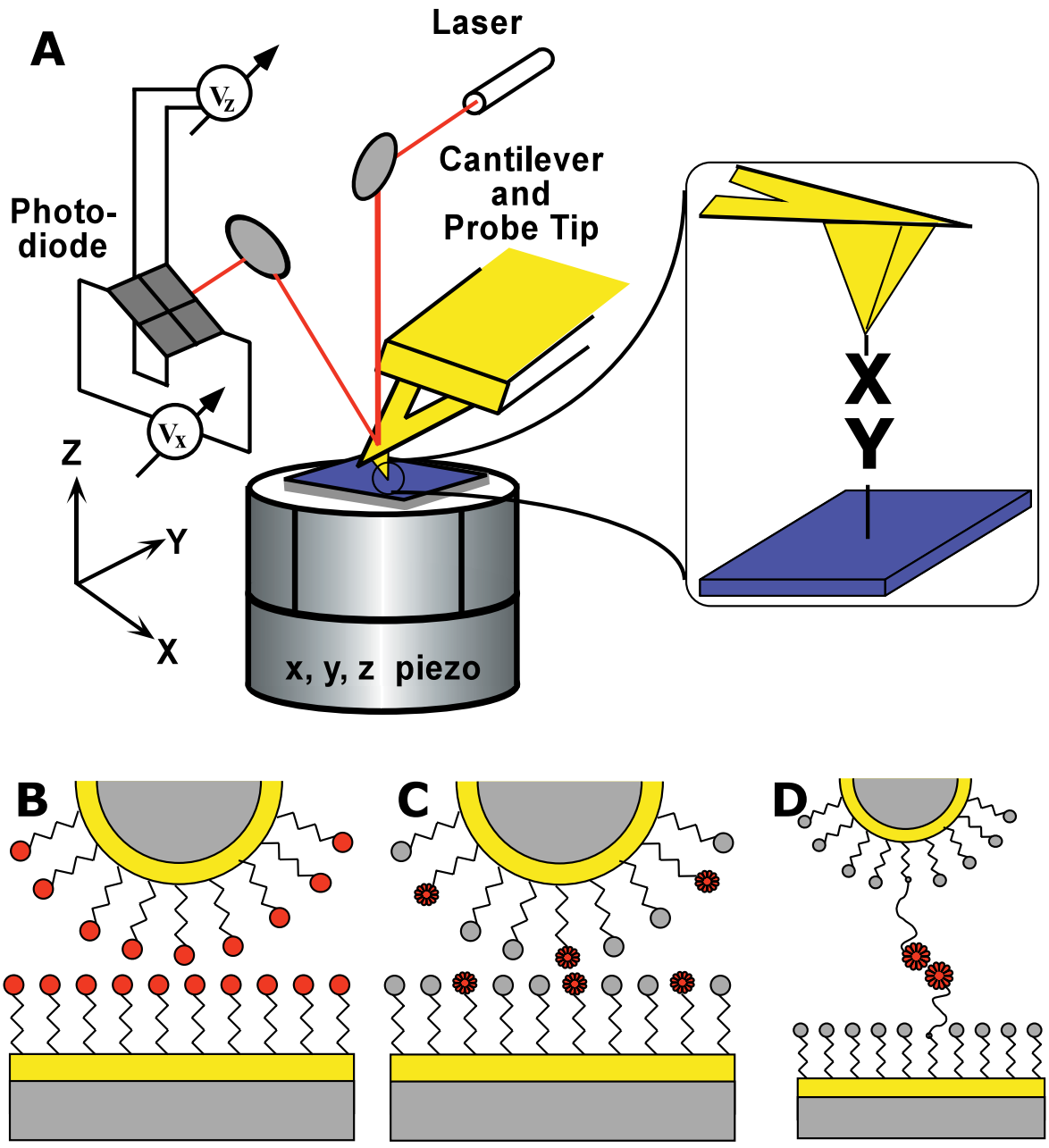

Figure 1: (**A**) Basic setup of a Chemical Force Microscopy experiment. A tip and a sample of the atomic force microscope are functionalized with specific chemical functionalities (inset). (**B-D**) Possible configurations of probe tip and sample functionalization. (B) All terminal functionalities bear the same chemical groups. (C) Active functional groups on the tip are "diluted" with inactive spacer molecules. (D) Interacting groups are attached to the surfaces of tip and sample through long flexible polymer tethers.

report!) the loading rates (i.e. the speed at which the cantilever loads the bond) used for the measurements. As we will discuss in the following sections, loading rate provides one of the critical dimensions in the parameter space of the CFM experiment. Third, the stochastic nature of bond ruptures at molecular scale dictates that researchers must always collect a sufficient number of individual rupture traces before they could determine the mean rupture force.

1.3 Interactions Between Basic Chemical Functionalities.

Lieber group showed that covalent modification of the AFM probes allowed them to distinguish between the interactions of basic types of functional groups [12, 25]. They showed that the interactions between hydrogen bonding -COOH groups are indeed stronger than the interactions between non-hydrogen-bonding groups such as CH_3 (Figure 2). Researchers quickly expanded these studies to include a large number of functional groups and solvents, and Table 1 summarizes some of these data (Reference [14] contains an expanded version of this table). However, even a quick look at these data shows that an idea of determining a defined bond strength which would be characteristic for a particular interaction is too simplistic. Interaction forces measured between the same functionalities in different solvents can differ by almost an order of magnitude, and, even more troubling, measurements performed by different research groups using similar probe functionalization in the same solvent can also produce different results. It is clear that interaction force can be influenced by many different parameters, and to understand the situation we need to consider the microscopic dynamics of the unbinding process.

2 Non-Covalent Bond Failure Under External Loading

2.1 Impact of Loading on a Potential Energy Surface

We begin by considering the general physical picture of a chemical bond subjected to mechanical loading by an external force (Figure 3). In this picture the bond is represented by a potential well of depth E_0. In reality, this potential well can comprise contributions from several distinct types of interactions, or several functional groups, as is often the case for the interactions of large functionalized AFM probes with flat surfaces. In the same generic picture the loading spring that exerts force on the bond is represented by another potential well with the minimum corresponding to the equilibrium position of the cantilever. Typ-

Functionality	Monolayer	Solvent	Adhesion (nN)	Reference
CH_3-CH_3	Silane, C_2	EtOH	0.4 ± 0.3	[26]
CH_3-CH_3	Silane, C_9	EtOH	0.7 ± 0.6	[26]
CH_3-CH_3	Silane, C_{14}	EtOH	2.4 ± 1.2	[26]
CH_3-CH_3	Silane, C_{18}	EtOH	3.5 ± 2.3	[26]
CH_3-CH_3	Thiol, C_{18}	EtOH	1.0 ± 0.4	[25]
CH_3-CH_3	Thiol, C_{12}	EtOH	2.3 ± 1.1	[27]
CF_3-CF_3	Silane, C_{10}	EtOH	15.4	[28]
CH_3-CF_3	Silane, C_{18}, C_{10}	EtOH	*repulsive*	[28]
CH_3-CH_3	Silane, C_{18}	$CF_3(CF_2)_6CF_3$	52	[28]
CF_3-CF_3	Silane, C_{10}	$CH_3(CH_2)_6CH_3$	21	[28]
CH_3-CH_3	Thiol, C_{12}	$CH_3(CH_2)_{14}CH_3$	0.07 ± 0.05	[27]
COOH-COOH	Thiol, C_{11}	$CH_3(CH_2)_{14}CH_3$	0.11 ± 0.02	[27]
COOH-COOH	Thiol, C_{11}	Hexane	0.95 ± 0.26	[29]
COOH-CH_3	Thiol, C_{11}, C_{18}	EtOH	0.3 ± 0.2	[25]
COOH-COOH	Thiol, C_{11}	EtOH	2.3 ± 0.8	[25]
COOH-COOH	Thiol, C_{11}	EtOH	0.27 ± 0.04	[27]
COOH-COOH	Thiol, C_{11}	PrOH	1.37 ± 0.26	[29]
CH_2OH-CH_2OH	Thiol, C_{11}	EtOH	0.18 ± 0.18	[27]
COOH-COOH	Thiol, C_{11}	Water	2.8 ± 0.2	[29]
COOH-COOH	Thiol, C_{11}	Water, $pH < 5$	7.0 ± 0.2	[30]
COOH-COOH	Thiol, C_{11}	Water, DI	2.3 ± 1.1	[27]
COOH-CH_2OH	Thiol, C_{11}	Water, $pH < 5$	1.1 ± 0.5	[30]
CH_2OH-CH_2OH	Thiol, C_{11}	Water, $pH < 5$	1.0 ± 0.2	[30]
CH_2OH-CH_2OH	Thiol, C_{11}	Water, DI	0.3 ± 0.05	[27]
CH_3-CH_3	Thiol, C_{18}	Water	60 ± 5	[30]
CH_3-CH_3	Thiol, C_{12}	Water	12.5 ± 4.4	[27]

Table 1: Interaction strength between AFM tips and samples functionalized with specific functional groups measured in different solvents.

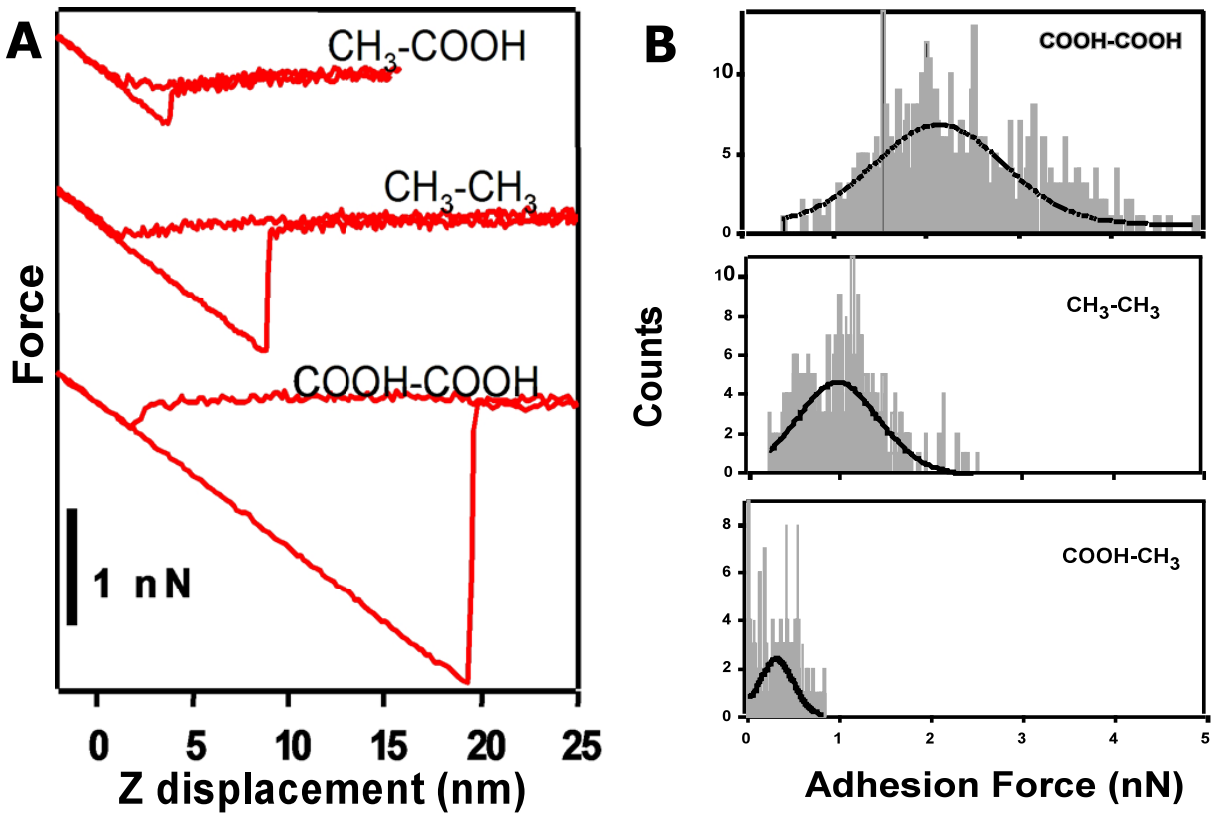

Figure 2: Specific interactions between basic chemical functionalities.(**A**) Representative force vs. distance traces recorded in ethanol between samples and tips functionalized with basic organic functional groups. From [12]. (**B**) Histograms of adhesion forces recorded between similar tip/sample pairs in ethanol. Solid lines indicate Gaussian fits to the data. From [25].

ically, this loading potential represents a parabolic potential of a cantilever spring. If the loading spring is very stiff, then its potential dominates the total interaction potential and forms the only minimum on the total potential energy surface of the bond-cantilever system. In this case the cantilever can simply trace the bond potential during the experiment. Unfortunately, sensitivity trade-off associated with using very stiff cantilevers effectively makes such measurements impractical; therefore direct tracing of the interaction potential is possible only for repulsive potentials, such as electrostatic repulsion in aqueous solutions. The topic of using CFM to probe electrostatic repulsion deserves a separate consideration, and we point the reader to the review papers on the topic [13, 14, 30]. In practice, the majority of the force spectroscopy measurements probes attractive interactions using soft springs, so we will concentrate on the analysis of these experiments.

Figure 3 shows that the loading with a soft spring creates a secondary minimum on the overall potential energy surface. Transitions between these two minima represent unbinding and rebinding events in this system. To complete the description, we need to add thermal fluctuations to the picture. Fluctuations are always an important element for the dynamics of these microscopic systems as they drive most of the transitions on the potential energy surface. Force microscopy measurements that concern us always happen in condensed phase; therefore it is reasonable to assume that these systems reach thermal equilibrium on a much faster timescale than the timescale for the unbinding or rebinding transition.

What role does external loading force play in determining the probability of the unbinding or rebinding transition? A quick look at the Figure 3 tells us that the presence of an external loading force potential lowers the barrier to the unbinding and raises (or creates) the barrier for rebinding and that these changes in turn modify the kinetic rates for barrier crossing. The exact amount of changes in the transition energy barriers depends on the exact geometry of the potential energy surface, yet the general physics remain similar: external force amplifies the rate of unbinding and retards the rate of rebinding.

These modifications to the rates of the fundamental transitions occurring in the system define two distinctly different kinetic scenarios. If the external force is high or the geometry of the potential energy surface is such that the rate of rebinding drops so low that rebinding happens at timescales beyond the experimental timescale, then unbinding will occur far from equilibrium. In this case, which is by far the most important for force spectroscopy measurements, the thermally-activated escape from the primary potential energy well will determine the bond rupture kinetics. If the applied force is low or if the potential energy surface is structured in such a way that rebinding still happens on the timescale comparable

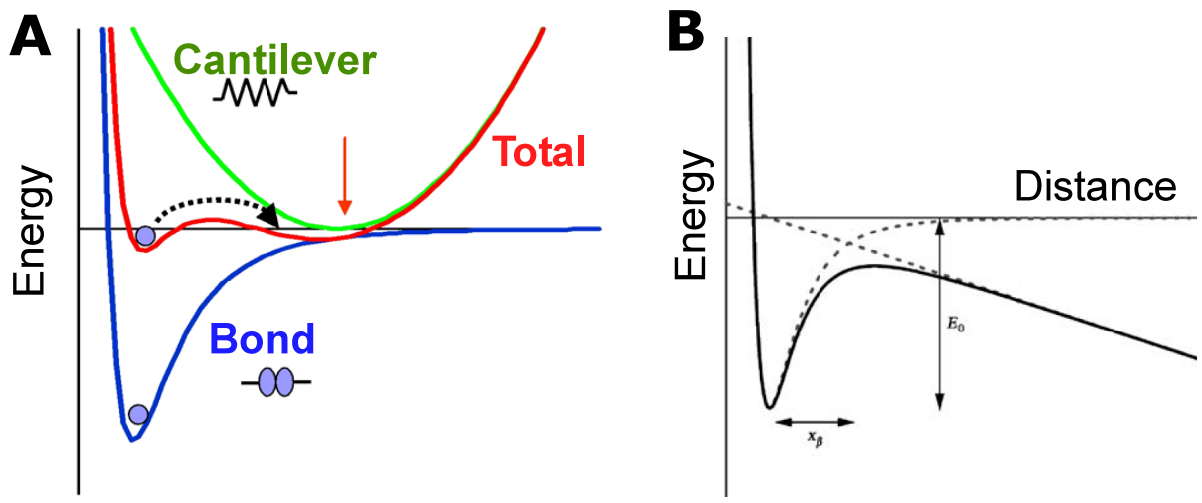

Figure 3: **A** A general energy diagram representing a chemical bond (blue) loaded by a parabolic Hookean spring (green) representing the AFM cantilever. The resulting potential energy surface is shown in red. **B**. Potential energy surface for a sharp energy barrier loaded by a weak spring

with the measurement timescale, then the unbinding occurs in near-equilibrium conditions and the kinetics of bond rupture is determined by the interplay between the thermally-activated unbinding and rebinding transitions. In practice, researchers rarely perform force spectroscopy measurements using constant load forces; instead loading force increases with time at a constant rate as the transducer pulls the AFM cantilever away from the sample at constant speed. In this case the *loading rate* becomes one of the most important parameters that determine the unbinding kinetics.

2.2 Non-Equilibrium Unbinding

The effect of the applied force on the unbinding and rebinding rates depends on the exact shape of the potential energy surfaces of the bond and the loading spring, yet we could quantify it for some simple cases. If a sharp potential energy well is loaded by a relatively weak spring, then we can assume that the loading force does not change appreciably over the barrier width distance and that we can replace the parabolic potential in Figure 3A with a linear potential (Figure 3B). G. Bell proposed a famous model that described the influence of applied force on the transition rates in this case; he postulated that external force F modulates the transition rate k_{unb} by a simple Boltzmann-weighted factor:

$$k_{unb}(F) = k^0_{unb} \cdot exp\left(\frac{Fx_\beta}{k_BT}\right) \tag{1}$$

where k^0_{und} represents the transition rate in absence of the external force and x_β is the characteristic distance to the transition state, or the "width of the potential". The rebinding rate is retarded in the same manner:

$$k_{reb}(F) = k^0_{reb} \cdot exp\left(\frac{-Fx^{reb}_\beta}{k_BT}\right) \tag{2}$$

here x^{reb}_β is the distance from the unbound state to the transition state. A quick look at this formula reveals that we could realistically hope to observe near-equilibrium unbinding only in the systems that feature very slow loading *and* small distances x^{reb}_β.

If we subject the bond to fast loading, or if the rebinding barrier is wide, then we can neglect the rebinding rate and only consider the unbinding kinetics. Evans and Ritchie solved the kinetic equations for this case and showed that the most probable binding force observed in these measurements will increase with the increase in the loading rate according to the following expression [31]:

$$F = \frac{k_BT}{x_\beta} ln\left(\frac{x_\beta}{k_BT \cdot k_{off}}\right) + \frac{k_BT}{x_\beta} ln(R_f) \tag{3}$$

where k_{off} is the unbinding rate constant in absence of applied force and R_f is the loading rate. This equation shows that in the non-equilibrium unbinding regime a bond does not possess a single characteristic strength; instead the measured bond strength is a strong function of the loading history of a bond. We could also use the plot of the measured interaction strength as a function of the loading rate (i.e. a *dynamic force spectrum*) to estimate the values of the bond off-rate (k_{off}) and the distance to the transition state x_β. We will discuss applications of this equation to Chemical Force Microcopy measurements throughout this article.

Before we consider this description, it is necessary to mention that historically the first framework for the description of the force spectroscopy experiments with AFM was based on the equilibrium continuum contact mechanics model, more specifically on the Johnson, Kendall, and Roberts (JKR) model [32]. Applications of this model to the force spectroscopy data analysis are described in detail in several reviews, specifically, we point the reader to references [13, 14, 33]. Several experimental studies demonstrated that JKR model provides an accurate description of rupture force scaling with the AFM probe radius [34] and tip-sample

surface interfacial free energy [33]. However, several factors severely limit the utility of the JKR model for the interpretation of force spectroscopy experiments: (1) JKR is a continuum model, which obviously poses serious problems for interpreting molecular-scale experiments; (2) JKR assumes contact-range interaction potential between the tip and sample surfaces, which sweeps under the rug most of the molecular-level details of the interactions. Recent simulations [35] showed that the processes in the tip-sample contact area deviate significantly from the description provided by various continuum contact mechanics models (although of all continuum models JKR model does provide the best description). Robbins and Luan recently used molecular simulations to test the limits of the contact mechanics description [36] and showed that it only provides a reasonable estimate of the contact area. Therefore JKR estimates are best to be limited to the estimating the tip-sample contact area (and the number of interacting groups) in the CFM experiment. For example, researchers used JKR models to estimate [25] that interactions of COOH-terminated surfaces in ethanol involve about 20 individual functional groups.

3 Equilibrium Unbinding in Multiple Bond Systems

Evans has published a brief analysis of the unbinding in the near-equilibrium regime [37]. He noted that in that case the force ceases to be a function of the loading rate, and instead the value of the bond rupture force is set by the rate constants for the unbinding and rebinding, the distances to the transition state from the bound and unbound states, and the stiffness of the probe. Therefore, we can expect that the rupture force will remain independent of the loading rate as the rate falls below a certain threshold value. As the loading becomes faster, the applied force begins to repress rebinding more and more, and the bond rupture will transition from the near-equilibrium regime back to the non-equilibrium regime where the rupture force will begin to increase with the loading rate.

Zepeda et al [38] observed such behavior in the CFM experiments where they measured binding forces between COOH-terminated AFM tips and COOH-terminated surfaces in ethanol (Figure 4). Note that the slope of the force spectrum in the non-equilibrium regime indicated an extremely narrow effective distance of 0.6 Åto the energy barrier. Zepeda et al. also observed a similar transitions for the interactions of a bare silicon nitride AFM tip with the mica sample surface.

Evans pointed out an interesting feature of the unbinding in the near-equilibrium regime. Since the measured binding force reflects both the unbinding and rebinding kinetics, the

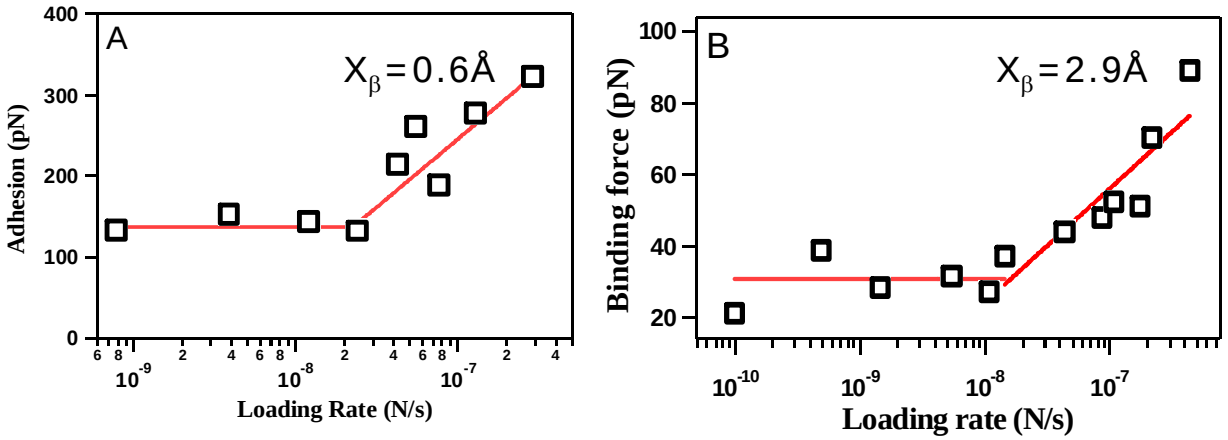

Figure 4: Dynamic force spectra for the interactions between (**A**) COOH-terminated AFM tip and COOH-terminated surface, and (**B**) Si_3N_4 tip and mica surface showing a transition from near-equilibrium unbinding to the non-equilibrium unbinding. From [38].

shape of the secondary "capture" well should also influence the measured forces. If we consider that capture well primarily represents the potential of a cantilever spring, we then arrive at a paradoxical conclusion that the measured value of binding force for the near-equilibrium unbinding should depend on the spring constant. Evans predicted that the measured binding force in the near-equilibrium regime should scale as the square root of the cantilever spring constant. To the best of our knowledge this prediction has not yet been tested in the experiment.

4 Solvation Barriers in Functional Group Interactions

4.1 Effect of Solvent on Adhesion Forces

Sinnia et. al. first noticed that measured adhesion forces between specific chemical groups are highly dependent on the solvent medium [27]. At first, this observation seems counterintuitive: the solvent molecules are likely squeezed out from the tip-sample gap during contact, and the solvent does not enter this gap until after the bond rupture. However, if we consider that after rupture the tip and sample surfaces immediately become solvated, it becomes clear that solvent must play an important role in stabilizing (or destabilizing) the unbound state, and thus must influence the kinetics of the bond rupture. Lieber and co-workers used continuum mechanics models and free energy arguments to provide the thermodynamic description

of the solvent effect on the adhesion forces [13, 33]. They used surface tension component theory [2] to rationalize results observed in ethanol and in water-methanol mixtures [33]. Nealey and Clear reported adhesion forces between CH_3-terminated probes and CH_3- and COOH-terminated siloxane surfaces in a range of solvents [39] and found good agreement between the measured work of adhesion for CH3/CH3 interface in a number of solvents and STC model predictions.

Vezenov et al. also observed [33] that adhesion forces measured in different solvents did not correlate with solvents polarity, or with cohesion energy of the solvent (Hildebrand parameter [40]). In contrast, STC model provided a good correlation. Use of methanol-water mixtures provided a simple way to generate similar solvents that span a large range of hydrogen bonding ability. Adhesion between non-polar functional groups increased monotonically with higher water content while force between polar hydrogen-bonding functional groups decreased compared to non-polar counterpart. Overall, surface tension component interpretation of the CFM data showed that competition between solvent-solvent interactions and solvent-surface interactions provides the main contribution to adhesion forces between organic functional groups in liquids.

4.2 Probing Entropic Solvation Barriers with Variable Temperature CFM

Noy and coworkers investigated the microscopic origins of these effects by measuring interaction forces between specific functional groups in different solvents as a function of temperature [16]. These experiments utilized a custom-built AFM chamber that gave researchers access to a wide range of temperatures [41]. Intuitively, we expect the binding force to decrease as the temperature increases and thermal fluctuations gain more energy to break the bonds. Surprisingly, researchers observed that for interactions between COOH-terminated surfaces in a polar, hydrogen-bonding solvent the interaction strength increased with the temperature (Figure 5A). Other hydrophilic functionalities also showed a similar counterintuitive behavior in polar solvents. Conversely, as researchers switched the medium to a non-polar solvent (hexane), the temperature trend reversed (Figure 5B). Qualitatively, this behavior originates from the large entropy loss that accompanies ordering of solvent molecules at the interfaces [16]. This negative entropy tends to destabilize the unbound state and cause the observed counterintuitive temperature dependence. In contrast, non-polar solvents do not tend to form ordered layers and thus do not contribute to these entropic solvation barriers.

Kinetic model equations provide a quantitative interpretation of this phenomenological picture. If we separate the energy barrier into enthalpic and entropic components, $E = \Delta H - T \cdot \Delta S$, and rearrange Equation 3, we can represent the temperature dependence of pull-off forces in a much more revealing form [16]:

$$F = \frac{\Delta H}{x_\beta} - T \cdot \frac{\Delta S}{x_\beta} - \frac{k_B T}{x_\beta} \cdot ln\left(\frac{k_B T}{\tau_0 R_f x_\beta}\right) \tag{4}$$

The first two terms in Equation 4 describe the enthalpic and entropic contributions to the bond strength, and the third term defines the contribution of thermal motion. In other words, the first two components describe the contribution from an energy barrier, and the third term, which is always negative, describes the "kinetic weakening" caused by thermal fluctuations that help the system to get over the activation barrier. The kinetic term in the Equation 4 always increases in magnitude as the temperature increases, and usually causes the expected decrease in the overall binding force. However, the entropic term can lead to either increase or decrease in the overall interaction force depending on the sign on the entropy change for the unbinding process. Therefore, for the cases when the energy barrier has a large entropy component (for example, in cases of solvent-mediated interactions) the bond strength could indeed increase with the temperature. The relative magnitude of the entropic and the kinetic terms in Equation 4 defines two regimes of bond rupture: (1) thermally-dominated kinetics where bond strength decreases with the temperature, and (2) barrier-dominated kinetics where the entropic term overwhelms the kinetic term and causes interaction strength to increase with the temperature. Furthermore, Equation 4 indicates that the entropic regime of unbinding exist only over a limited range of temperatures. As the temperature increases, the kinetic term which increases as $T \cdot ln(T)$ will always overwhelm the entropic term which increases only linearly. For the entropic barriers caused by the ordering of the solvent molecules at the surface this cross-over point simply corresponds to the situation when the thermal motion becomes too strong and overwhelms molecular ordering in the solvent layers.

Another non-trivial effect arises if we consider that these two terms scale differently with the system size. It is clear that the entropic term is significant only when the tip-sample contact area exceeds a certain critical size. This effect is qualitatively similar to the size-induced cross-over common for hydrophobic molecule association in water [42]. Researchers have calculated that for a typical CFM experiment this crossover could happen when the radius of the probe tip falls below 5 nm [16]. Current progress in fabrication of ultra-sharp AFM probes and especially the advent of carbon nanotube AFM tips [43, 44] ofers an op-

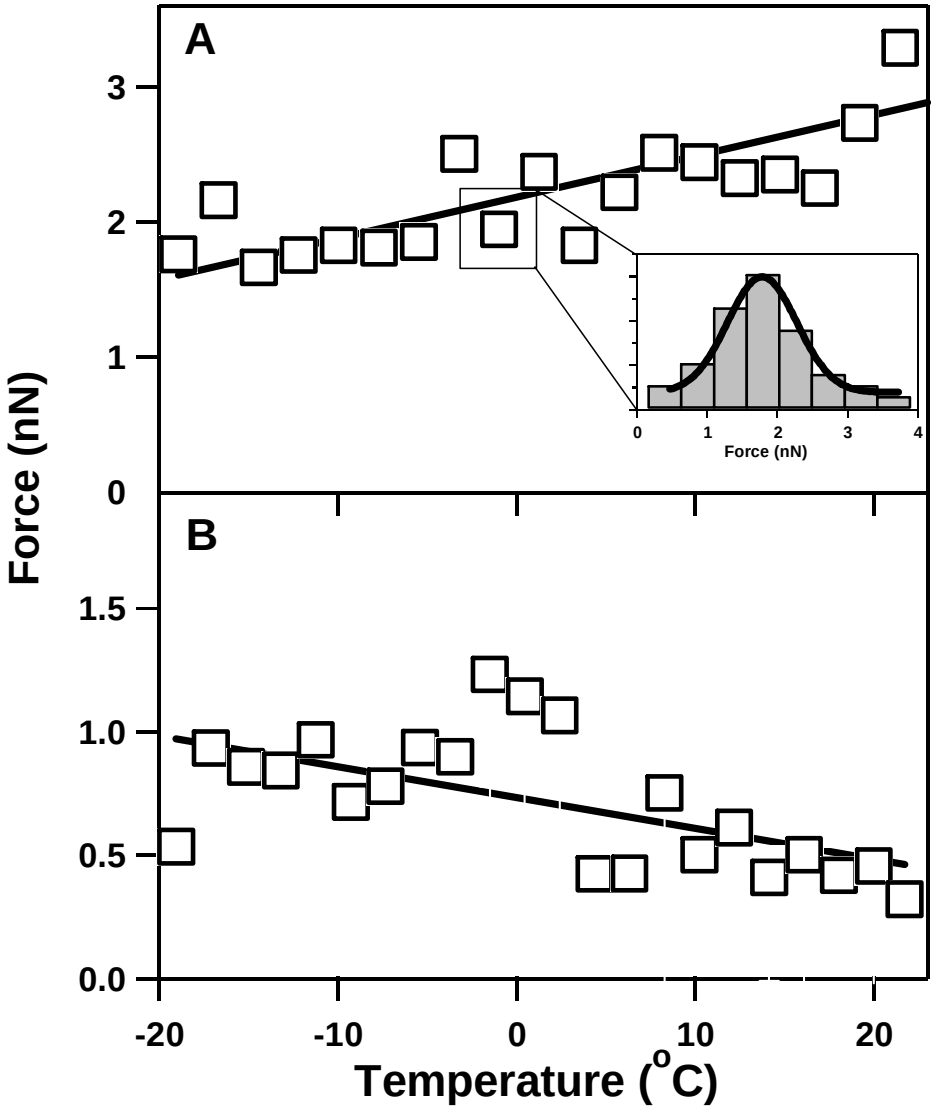

Figure 5: Variable-Temperature Chemical Force Microscopy. (**A**) Binding force as a function of temperature for interactions of COOH-modified probe and sample in ethanol. Inset shows a binding force histogram at one temperature point. (**B**) Binding force as a function of temperature for the interactions of COOH-modified probe and sample in hexane. From [16].

portunity for the experimental verification of this prediction. Overall, it is abundantly clear that solvent medium plays a key role in shaping the interactions between nanoscale ensembles of functional groups, and that solvation is one of the critical factors that determined the magnitude of the forces measured in the CFM experiments that probe forces between ensembles of chemical functionalities.

5 Near-Equilibrium Unbinding: Chemical Force Microscopy of Duplex DNA Interactions

Binding forces between DNA strands as well as mechanical properties of the double helix have always been an interesting topic, motivated primarily by the overarching importance of DNA in the storage and transfer of biological information. Not surprisingly, soon after Gaub's group demonstrated the possibility of using AFM to detect biological interactions [15, 45], Lee and co-workers used AFM to measure specific recognition interactions between 20 bp-long DNA oligomers [46]. Unfortunately, the DNA sequence used in these experiments allowed for some slipping of the complementary strands against each other, and as a consequence researchers have observed distinct clusterings of forces which they attributed to complementary interactions between overlapping regions of DNA of different length produced during such slipping. In addition, elastic linkers used in these experiments precluded observation of the mechanical signature of DNA stretching. Lieber and coworkers [20] have approached this problem differently and constructed two complementary "non-slipping" 14-mer DNA sequence that formed a double helix only in a unique orientation. They have also attached the DNA oligomers directly to the surface of a thiol monolayer terminated in passivating -OH functionalities (Figure 6, insert). This configuration provided a rigid "handle" to apply force directly to the double helix, while simultaneously minimizing non-specific probe-sample interactions.

Researchers used this system to detect and characterize complementary interactions between one and two individual complementary DNA strand pairs (Figure 6). Moreover, the "diluted monolayer" attachment configuration(see Figure 1B) allowed them to detect the mechanical signature corresponding to the structural transition in individual DNA duplexes. This transition to an overstretched S-DNA form (see inset on the Figure 7A for a graphic representation) had been previously observed in macroscopic length DNA in the experiment [47, 48], as well as in computer simulations [49, 50]. A puzzling feature of the stretching transition observed in the AFM experiment was a relatively high value of 120 pN of the force

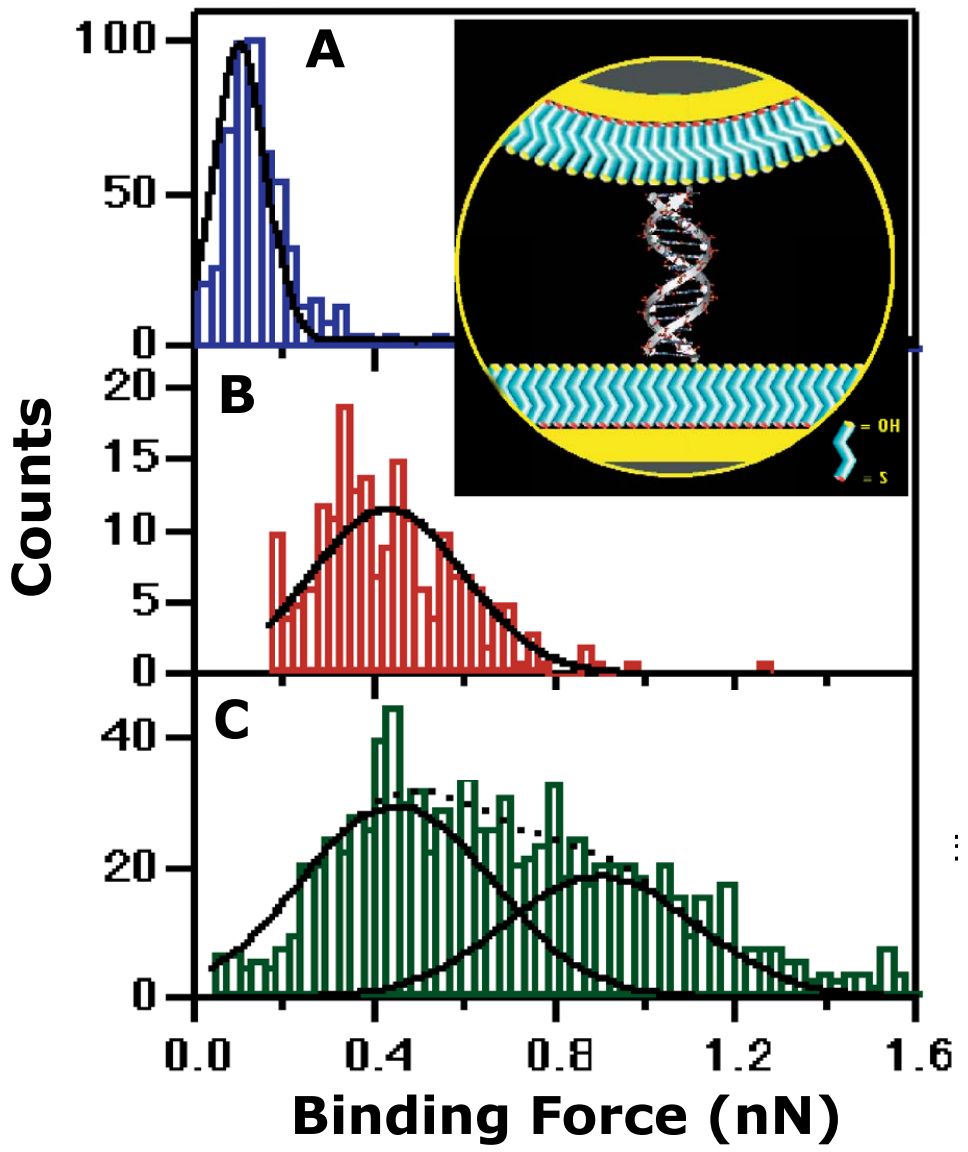

Figure 6: Histograms of the binding force values obtained from multiple measurements between gold surfaces functionalized with the DNA oligonucleotides (inset). (A) Noncomplementary pair. (B, C) Complementary pair. Peaks corresponding to non-complementary interactions (less than 150 pN) were removed from (B) and (C) for clarity. The bimodal distribution in (C) reflects the presence of two active DNA strands on the AFM tip. Solid lines in (A) and (B) represent best fits to a Gaussian distribution. The dashed line in (C) is the best fit to a sum of the two Gaussian distributions indicated by solid lines. From [20].

plateau that corresponded to the transition to S-DNA (Figure 7B). In comparison, equilibrium measurements on the macroscopic length DNA molecules have consistently reported plateau force of 70 pN; Gaub and co-workers also reported a similar plateau force values for stretching macroscopic DNA molecules with AFM [10].

Noy has subsequently re-analyzed the data using equilibrium potential reconstruction technique based on Jarzynski equality [51, 52] and demonstrated that the deviation in the plateau force from the equilibrium value reflects energy dissipation occurring in the AFM measurement [53]. Indeed, when the reconstruction procedure removed the dissipation effects, the plateau force dropped to 80pN, which was much closer to the equilibrium value. Perhaps more important, the depth of the reconstructed potential energy well matched the equilibrium DNA melting enthalpy value to within 1% accuracy. While such close correlation was likely fortuitous (given the customary 10% error introduced by the spring constant calibration), these results demonstrate the validity of chemical force microscopy approach for single-molecule level determination of the thermodynamic parameters of molecular interactions. We stress that "diluted monolayer" configurations present perhaps the only opportunity for applying such analysis to the single molecule force spectroscopy measurements, as bond rupture in the systems using tethered configurations always occurs far from equilibrium (see discussion in the following section, as well as in references [37, 54], and thus exhibit very high levels of energy dissipation which make the potential energy reconstruction process impractical. In these cases researchers should use dynamic force spectroscopy protocol to determine kinetic parameters of the interaction, as Strunz et al. demonstrated for unbinding of 10-30bp DNA duplexes attached to the AFM probe by 30-nm PEG tethers [55].

6 Non-Equilibrium Bond Rupture: Chemical Force Microscopy of Single and Multiple Biological Bonds

6.1 Dynamic strength of single and multiple biological bonds

As we discussed in the previous sections, attaching the interacting molecules to flexible tethers provides multiple advantages for detecting specific biological interactions. Tethers provide spatial separation between the specific and non-specific interactions (see Figure 8). Researchers used tether-based configurations to detect specific interactions between receptor-ligand pairs [56], and protein-antibody interaction that provides a targeting interaction for

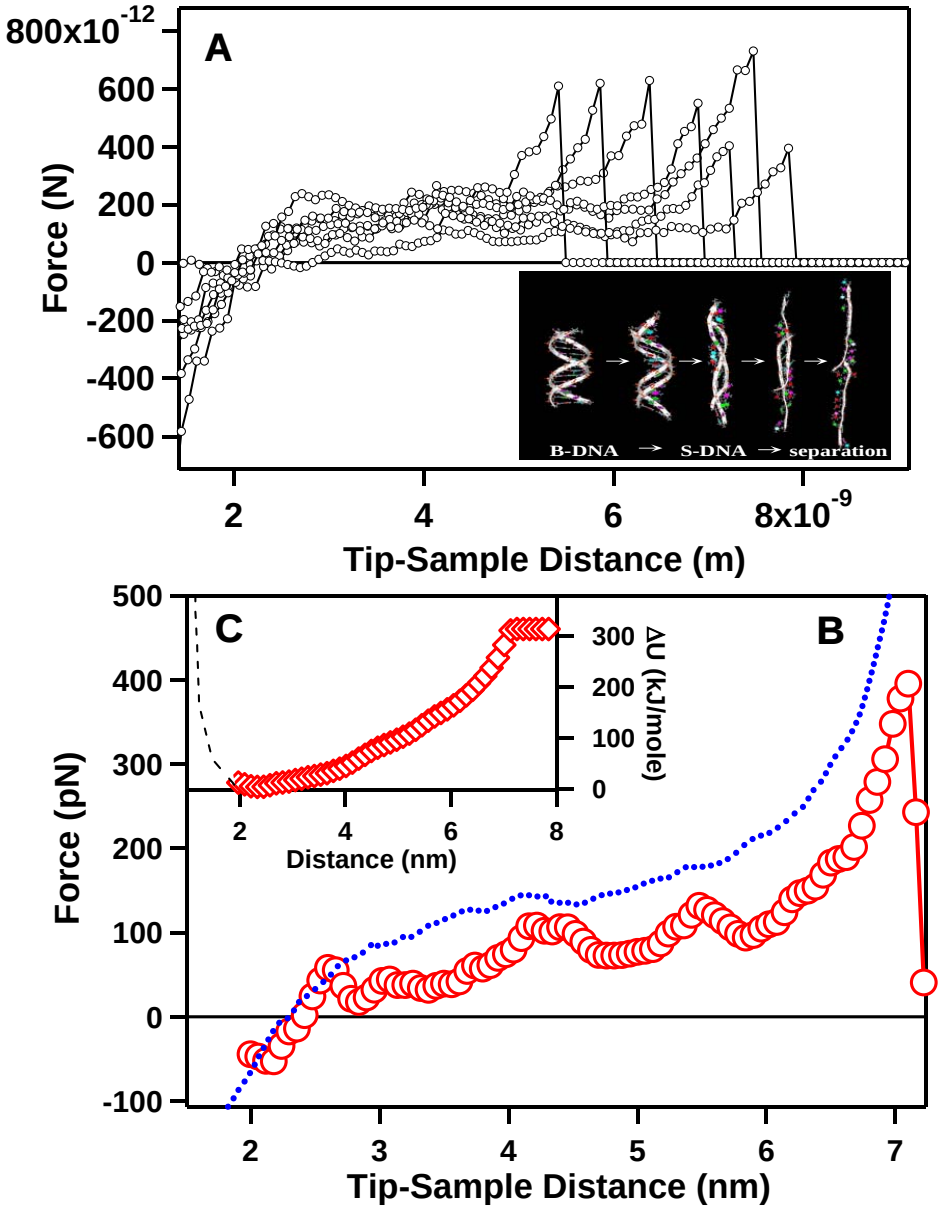

Figure 7: (**A**) Representative individual force vs extension traces showing stretching and breaking of a 14-mer DNA duplex. Inset shows snapshots of a computer simulation of the stretching process (simulation courtesy Dr. R. Lavery, Inst. Curie, France). (**B**) Comparison of an average force vs. extension trace (dashed blue line) with the equilibrium force vs. extension trace (red circles) reconstructed using Jazynski equation. (**C**) Reconstructed interaction potential. From [53].

multivalent immunotherapeutic drugs [21]. However, the price for these advantages involves introduction of a non-linear spring representing the entropic elasticity of the polymer tether in series with the chemical bond of interest. Such configuration has profound consequences on the loading of the bond as well as on the potential energy surface for the system.

The elastic response of a polymer tethers typically starts with a very soft initial region, which then quickly stiffens as the polymer extension approaches its contour length. The entropic elasticity of the polymer chain that dominates this initial region is typically described either by the Freely-Jointed-Chain (FJC) model for a flexible polymer of by the Worm-Like-Chain (WLC) model for a stiffer polymer. Bustamante and co-workers used an interpolation formula [57] that describes the force-extension relationship for the WLC polymer of the contour length L_0 and persistence length λ:

$$F(x) = \frac{k_B T}{\lambda}\left[\frac{1}{4}\left(1 - \frac{x}{L_0}\right) - \frac{1}{4} + \frac{x}{L_0}\right] \tag{5}$$

Researchers have successfully used these approximation to describe experimental force vs. extension relationships observed for DNA, polypeptide chains, polysaccharides and other biological polymers [7, 58, 10, 59, 60, 61, 62]. One polymer that deserves a special mention is polyethyleneglycol (PEG) chain, mainly because PEG turns out to be an ideal tether for CFM experiments on biological molecules: it has low non-specific adhesion to biological surfaces [63], and it is widely available in different lengths and conjugation-ready chemical terminations.

Oesterhelt and coworkers [64] analyzed the configuration of PEG polymers in solution and showed that the length of a PEG polymer during stretching in apolar solvents follows closely the prediction of an FJC model. However, stretching of PEG chains in water leads to a structural transition in the polymer. Molecular dynamics simulations and the experimental measurements suggest that this transition represents breakage of supramolecular helical formations stabilized by water bridges [64]. Applied forces larger than 100 pN break these water bridges, lengthening the polymer. Researchers proposed a model that accounts for this transition by allowing each PEG segment to exist in two states, a compact (helical) state and extended (planar) state. The equilibrium population of these two states is thermally distributed, and tilted towards the compact state at zero force and towards the extended state at high force. If we consider N_t identical PEG tethers (each containing N_m monomers), then the force-extension relationship will be given by [64]:

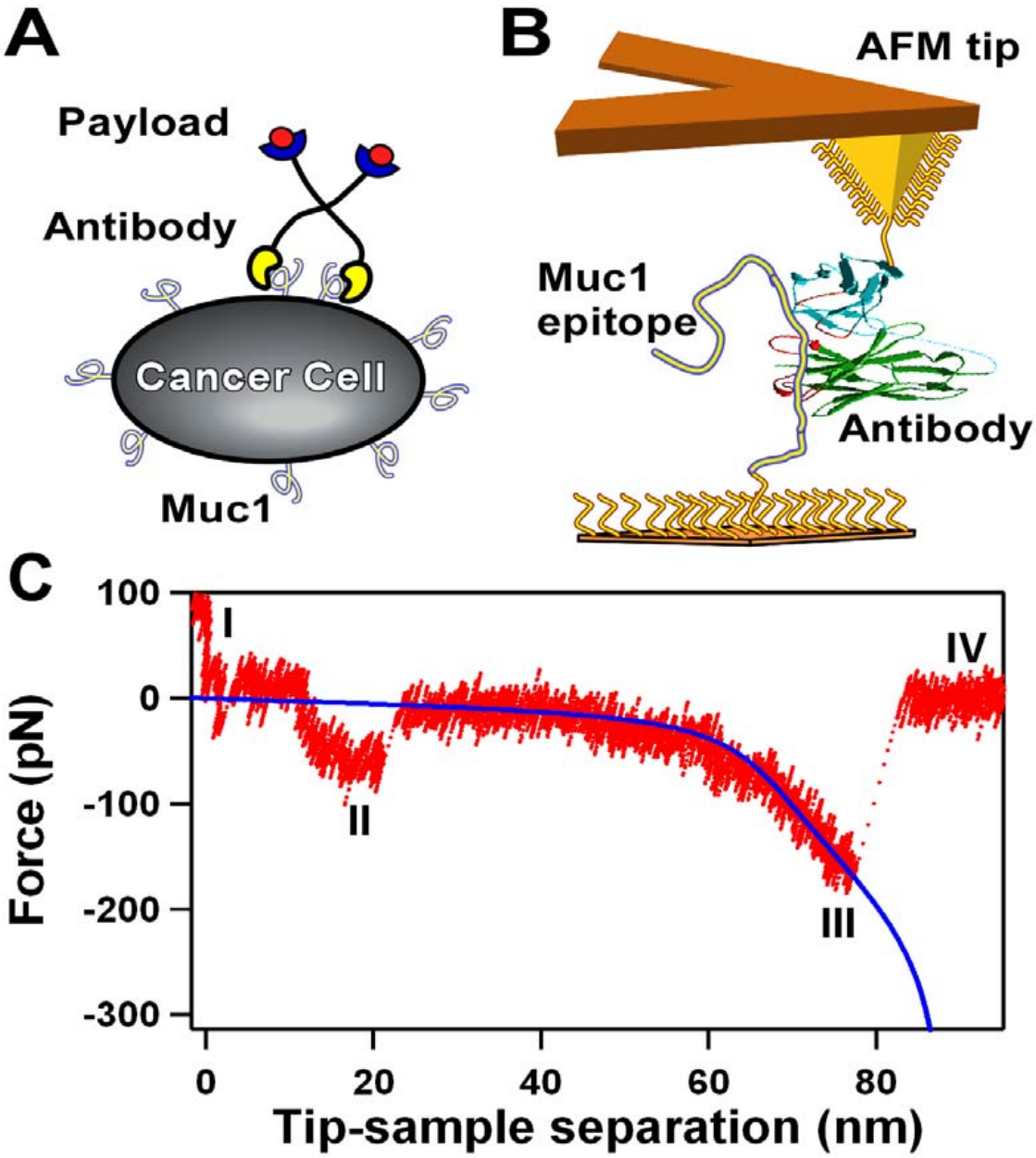

Figure 8: (**A,B**) A tethered-ligand based system that mimics interactions of a multivalent radioimmunotherapeutic agent with the target receptor on the surface of a cancer cell (Part A). Part B shows an equivalent force spectroscopy measurement in which the AFM tip is connected to an antibody and a sample surface is connected to the target MUC1 peptide with flexible PEG tethers. **C**. Representative force vs. separation trace showing repulsive interactions region (**I**), non-specific interactions region (**II**), specific interaction region (**III**), and free cantilever deflection region (**IV**). The blue line indicates an extended Freely Jointed Chain model fit for the tether stretching in the specific interactions region.

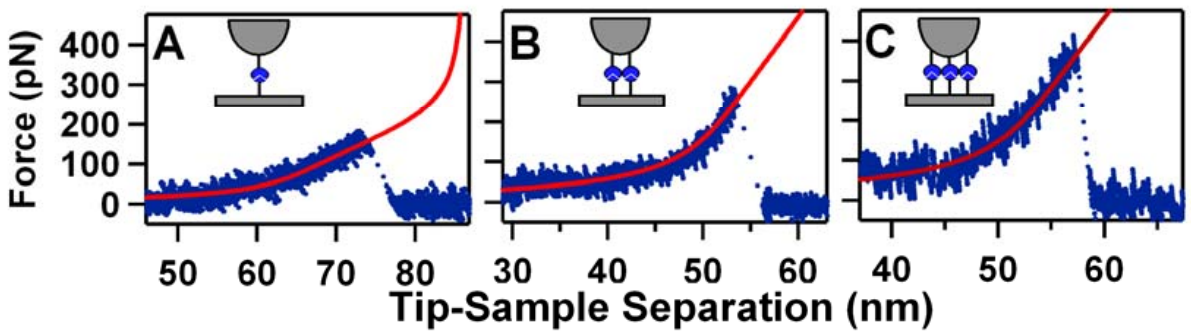

Figure 9: Individual tether stretching traces before specific bond rupture events showing rupture of one (**A**), two (**B**) and three (**C**) protein-antibody bonds. Red lines indicate extended FJC model fits for the corresponding number of traces. Tether contour length was the only fitting parameter used to generate the model fits. From [21].

$$L(F_t, N_t) = L_c(F_t, N_t) \cdot \left[coth\left(\frac{FL_k}{N_t k_B T}\right) - \frac{N_t k_B T}{FL_k} \right] + \frac{N_m F}{N_t K_s} \tag{6}$$

Here, L_k is the Kuhn length, K_s is the molecular bond stiffness, and $L_c(F, N_t)$ represents a force-dependent contour length which is simply a sum of the lengths of the compact and extended monomers in the chain at a given force F. This model provides an excellent description of the elasticity of one and several PEG tethers connected in parallel to the AFM tip and surface (Figure 9).

6.2 Dynamic Force Spectroscopy of Tether-Based Systems

When the cantilever applies force to the bond through a polymer linker, the capture potential always contains a very shallow region near the minimum; as the result, the distance from the unbound state to the transition state in this case will always be large. As predicted by Equation 2, such potential energy surface geometry makes rebinding negligible. Therefore, unbinding in tether-based systems always happens as a non-equilibrium process, and thus requires full kinetic treatment [31, 54]

In this case the experimental strategy is to probe the exponential dependence of the rupture force on the loading rate (as predicted by the Equation 3). It is important to point out that addition of the entropic tether spring to the system causes non-linear loading of the bond. Fortunately, Gaub and co-workers demonstrated that using an instantaneous loading rate at the moment of rupture produces dynamic force spectra that are a reasonable approximation of the true dynamic force spectra [65]. This approach allows researchers to

obtain dynamic force spectra and extract kinetic parameters for individual single [65], and multiple [21] bonds in tether-based systems (Figure 10).

These experiments also raise the possibility of direct experimental testing of the the kinetic model for the strength of multiple bonds developed by Williams [66], who analyzed rupture of multiple identical bonds and showed that the measured rupture force, f^*, will scale with the number of bonds, N_B, and loading rate, r_f, as:

$$r_f = k_{off} \frac{k_B T}{x_\beta} \left[\sum_{i=1}^{N_B} \frac{1}{i^2} exp\left(-\frac{f^* x_\beta}{i k_B T} \right) \right]^{-1} \tag{7}$$

where x_β is the characteristic bond width, and k_{off} is the thermodynamic off rate for a single bond.

Noy and co-workers demonstrated that dynamic force spectra for the multivalent protein-antibody interactions indeed follow the predictions of this model (Figure 10. Interestingly, these results directly contradict the common assumption that the strength of the multiple bond is just a linear combination of the strength of individual bonds. This assumption even served as a basis for a published method of using Poisson statistics analysis for extracting the strength of a single bond from multiple bond strength measurements [29]. Kinetic model [66], as well as experimental measurements [67] prove that the true bond strength does not scale linearly with the bond number; therefore researchers should avoid using the Poisson statistics-based technique for data analysis and instead must use the full kinetic description.

7 Chemically-Sensitive Imaging with Functionalized AFM Probes

The description of Chemical Force Microscopy would not be complete without mentioning the use of functionalized AFM probes for specific mapping of the surface functionalities on the nanometer scale. This topic wholly deserves a separate review; therefore we provide only a cursory outline of the main issues and techniques. The most straightforward application of CFM to mapping of the surface functionalities would be to use a functionalized AFM tip to construct a 2-D map of adhesion forces. Some of these measurements relied Pulsed Force Mode imaging approach [68] that allowed high-speed collection of tip-sample adhesion values at a rate about 1 kHz (see [69]); however, the extremely high probe travel speeds inherent for these experiments probably pushed the interaction very far into the kinetic regime. Accurate interpretation of the pulsed force mode images should require effective

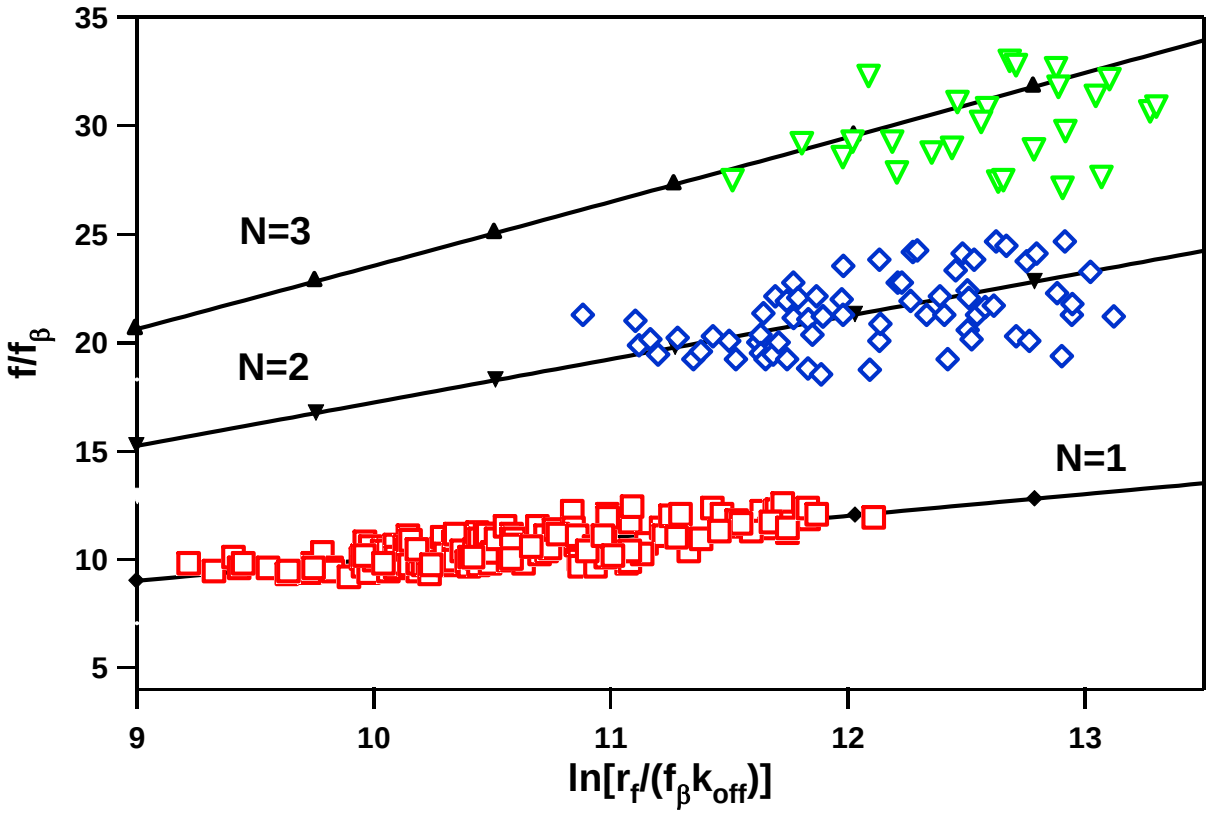

Figure 10: Normalized dynamic force spectra for the rupture of one (red squares), two (blue diamonds), and three (green triangles) MUC1-antibody bonds compared with the prediction of the uncorrelated multiple bond rupture model. Solid lines represent the results of the numerical solutions of the Equation 7 for N=1, 2, and 3. No fitting parameters were used to generate the theoretical curves. From [21].

control over the loading rate, which in that case involves significant technical difficulties.

Adhesion force collection at "normal" rates [70] pitted researchers against the inherent slow speed and large data volumes that such procedure requires, and therefore caused them to seek alternative approaches. Early on, Lieber and co-workers noticed that lateral (friction) forces measured using functionalized AFM tips correlate with the normal forces measured with the same probes [25]. This observation lead them to introduce the concept of chemically-specific lateral force imaging [12]. Later, the same group observed that the cantilever phase lag measured during tapping mode imaging (Figure 11) also correlates with the tip-sample interaction strength [71]. Later, Cleveland and co-workers showed that energy dissipation in the tip-sample junction region provided the true origin of the phase lag in tapping mode imaging. Therefore, a straightforward interpretation of tapping mode images collected with functionalized AFM tips is correct only if the contribution from other dissipation sources (i.e. viscoelastic effects) is small.

Recently, researchers reported several successful attempts to map specific interactions using AFM tips functionalized with specific molecules attached to flexible polymer tethers. Hinterdorfer and colleagues [72, 73] used an antibody attached to a short polymer tether to the end of the AFM tip and showed that specific interactions of the antibody with lysozyme molecules allowed them to map lysozyme locations of the sample surface with the claimed positional accuracy of 1.5 nm. Joselevich and co-workers recently presented an interesting modification of this approach where they used non-linear elasticity of the polymer tether coupled with the higher-harmonic detection in tapping mode scanning to map locations of the specific tip-sample interactions [74].

8 Outlook

Development of the experimental methods of measuring intermolecular interactions with AFM is remarkable for several reasons. First, these techniques allowed direct exploration of the role that different functionalities, solvents and environmental variables play in shaping the strength of intermolecular interactions. Chemical Force Microscopy approach in particular, turned out to be very effective in exploring some of these factors. Second, CFM studies clearly debunked the naive notion that intermolecular interaction strength is determined only by the nature of the interacting groups. These studies showed that the interaction strength between two chemical species must always considered in context of the environment surrounding these species, and, particularly the solvent medium, which plays a critical role in

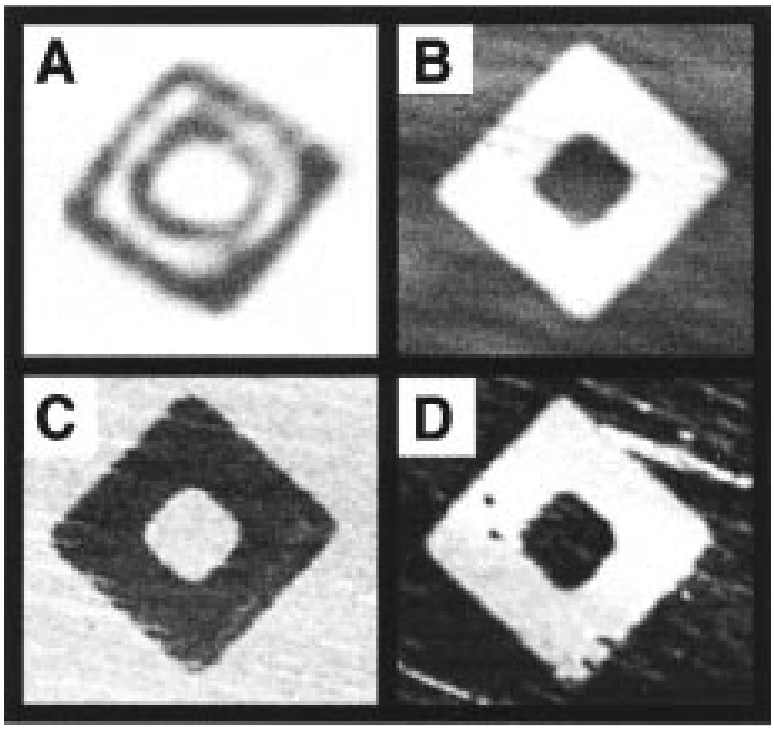

Figure 11: (**A**) Condensation figure obtained for a patterned self-assembled monolayer with CH_3- and COOH-terminated regions. Water droplets condense on the COOH-terminated regions and appear as a dark ring in this optical micrograph. (**B**) Friction map of a similar size area obtained with a COOH-terminated tip. Light and dark areas correspond to the regions of high and low friction, respectively. (**C, D**) Phase lag maps of the same sample taken with (C) a COOH-terminated tip and (D) a CH_3-terminated tip. Darker regions correspond to greater phase lag. All images are $25 \times 25 \mu m$. The contrasts in (B) and (C) and (D) correspond to friction differences of 25 nN and phase variations of 9° and 4°, respectively. From [71].

shaping intermolecular interactions in condensed phases.

Furthermore, the emerging kinetic view of the intermolecular interactions introduced a completely new paradigm for understanding these interactions. Kinetic model showed that the measured interactions strength depends not only on the energy landscape of the system, but also on the loading history prior to the bond break-up. This new paradigm refocused our attention to the energy landscape as a fundamental characteristic of the interaction. Moreover, the Dynamic Force Spectroscopy approach derived from the kinetic model allowed direct characterization of the potential energy barrier geometry. Further investigations of the interactions in different systems, especially interactions between biomolecules, will uncover many interesting characteristics of intermolecular potentials. These studies have the potential to reveal for the first time a true picture of the energy landscapes in complex chemical and biological systems.

9 Acknowledgement

This work was performed under the auspices of the U.S. Department of Energy by the University of California, Lawrence Livermore National Laboratory under Contract W-7405-Eng-48.

References

[1] Birdi, K. S. *Handbook of surface and colloid chemistry;* CRC Press: Boca Raton, Fla., 1997.

[2] van Oss, C. J.; Chaudhury, M. K.; Good, R. J. *Chem. Rev.* **1988,** *88,* 927-41.

[3] Israelachvili, J. *Intermolecular and Surface Forces;* Academic Press: New York, 1992.

[4] Israelachvili, J. *Acc. Chem. Res.* **1987,** *20,* 415-21.

[5] Israelachvili, J. N.; McGuiggan, P. M. *Science* **1988,** *241(4867),* 795-800.

[6] Ashkin, A.; Dziedzic, J. M.; Bjorkholm, J. E.; Chu, S. *Optics Lett.* **1986,** *11,* 288-90.

[7] Bustamante, C.; Macosko, J. C.; Wuite, G. J. L. *Nature Rev. Molec. Cell Biol.* **2000,** *1,* 130-136.

[8] Binnig, G.; Quate, C. F.; Gerber, C. *Phys. Rev. Lett.* **1986,** *56,* 930-3.

[9] Weisenhorn, A. L.; Hansma, P. K.; Albrecht, T. R.; Quate, C. F. *Appl. Phys. Lett.* **1989,** *54,* 2651-3.

[10] Clausen-Schaumann, H.; Seitz, M.; Krautbauer, R.; Gaub, H. E. *Curr. Opin. Chem. Biol.* **2000,** *4,* 524-530.

[11] Albrecht, T. R.; Akamine, S.; Carver, T. E.; Quate, C. F. *J. Vac. Sci. Technol. A.* **1990,** *8,* 3386-96 Using Smart Source Parsing.

[12] Frisbie, C. D.; Rozsnyai, L.; Noy, A.; Wrighton, M.; Lieber, C. *Science* **1994,** *265,* 2071.

[13] Noy, A.; Vezenov, D.; Lieber, C. *Ann. Rev. Mat. Sci.* **1997,** *27,* 381-421.

[14] Vezenov, D. V.; Noy, A.; Ashby, P. *J. Adh. Sci. Tech.* **2005,** *19,* 313-364.

[15] Florin, E. L.; Moy, V. T.; Gaub, H. E. *Science* **1994,** *264,*.

[16] Noy, A.; Zepeda, S.; Orme, C. A.; Yeh, Y.; De Yoreo, J. J. *J. Am. Chem. Soc.* **2003,** *125,* 1356 - 1362.

[17] Schonherr, H.; van Os, M. T.; Forch, R.; Timmons, R. B.; Knoll, W.; Vancso, G. J. *Chem. Mater.* **2000,** *12,* 3689-3694.

[18] Schonherr, H.; Hrushka, Z.; Vancso, G. *Macromolecules* **1997,** *31,* 3679-3685.

[19] Hillborg, H.; Tomczak, N.; Olah, A.; Schonherr, H.; Vancso, G. J. *Langmuir* **2004,** *20,* 785-794.

[20] Noy, A.; Vezenov, D.; Kayyem, J.; Meade, T.; Lieber, C. *Chemistry & Biology* **1997,** *4,* 519-527.

[21] Sulchek, T. A.; Friddle, R. W.; Langry, K.; Lau, E. Y.; Albrecht, H.; Ratto, T. V.; DeNardo, S. J.; Colvin, M. E.; Noy, A. *Proc. Natl. Acad. Sci. USA* **2005,** *102,* 16638-16643.

[22] Cleveland, J. P.; Manne, S.; Bocek, D.; Hansma, P. K. *Rev. Sci. Instr.* **1993,** *64,* 403-405.

[23] Sader, J. E.; Larson, I.; Mulvaney, P.; White, L. R. *Rev. Sci. Instr.* **1995,** *66,* 3789-98.

[24] Hutter, J. L.; Bechhoefer, J. *Rev. Sci. Inst.* **1993,** *64,* 1868-73 Using Smart Source Parsing.

[25] Noy, A.; Frisbie, C. D.; Rozsnyai, L. F.; Wrighton, M. S.; Lieber, C. M. *J. Am. Chem. Soc.* **1995,** *117,* 7943-7951.

[26] Nakagawa, T.; Ogawa, K.; Kurumizawa, T.; Ozaki, S. *Japan. J. Appl. Phys., P. 2 (Lett.)* **1993,** *32,* L294-6.

[27] Sinniah, S.; Steel, A.; Miller, C.; Reutt-Robey, J. *J. Am. Chem. Soc.* **1996,** *118,* 8925-8931.

[28] Nakagawa, T.; Ogawa, K.; Kurumizawa, T. *J. Vac. Sci. Technol. B, Microelectron. Nanometer Struct.* **1994,** *12,* 2215-18.

[29] Han, T.; Williams, J.; Beebe, T.P., J. *Anal. Chim. Acta* **1995,** *307,* 365-376.

[30] Vezenov, D.; Noy, A.; Rosznyai, L. F.; Lieber, C. M. *J. Am. Chem. Soc.* **1997,** *119,* 2006-2015.

[31] Evans, E.; Ritchie, K. *Biophys. J.* **1997,** *72,* 1541-1555.

[32] Johnson, K. L.; Kendall, K.; Roberts, A. D. *Proc. Royal Soc., A.* **1971,** *324,* 301-13.

[33] Vezenov, D. V.; Zhuk, A. V.; Whitesides, G. M.; Lieber, C. M. *J. Am.Chem. Soc.* **2002,** *124,* 10578-10588.

[34] Skulason, H.; Frisbie, C. D. *Langmuir* **2000,** *16,* 6294-6297.

[35] Patrick, D. L.; Flanagan, J. F.; Kohl, P.; Lynden-Bell, R. M. *J. Am. Chem. Soc.* **2003,** *125,* 6762-6773.

[36] Luan, B.; Robbins, M. O. *Nature* **2005,** *435,* 929-932.

[37] Evans, E. *Ann. Rev. Biophys. Biomol. Struct.* **2001,** *30,* 105-128.

[38] Zepeda, S.; Yeh, Y.; Noy, A. *Langmuir* **2003,** *19,* 1457-1461.

[39] Clear, S.; Nealey, P. *J. Coll. Interf. Sci.* **1999,** *213,* 238-250.

[40] Hildebrand, J.; Scott, R. *Regular Solutions;* Prentice-Hall: Englewood Cliffs, N.J., 1962.

[41] Zepeda, S.; Yeh, Y.; Orme, C. A. *Rev. Sci. Instr.* **2001,** *72,* 4159-4163.

[42] Chandler, D. *Nature* **2005,** *437,* 640-647.

[43] Hafner, J. H.; Cheung, C. L.; Oosterkamp, T. H.; Lieber, C. M. *J. Phys. Chem. B* **2001,** *105,* 743-746.

[44] Wong, S. S.; Joselevich, E.; Woolley, A. T.; Cheung, C. L.; Lieber, C. M. *Nature* **1998,** *394,* 52-55.

[45] Moy, V. T.; Florin, E. L.; Gaub, H. E. *Science* **1994,** *266,* 257-9.

[46] Lee, G. G. U.; Chrisey, L. L. A.; Colton, R. R. J. *Science* **1994,** *266,* 771-773 0036-8075.

[47] Smith, S. B.; Cui, Y.; Bustamante, C. *Science* **1996,** *271,* 795.

[48] Cluzel, P.; Lebrun, A.; Heller, C.; Lavery, R.; Viovy, J.-L.; Chatenay, D.; Caron, F. *Science* **1996,** *271,* 792.

[49] Konrad, M. W.; Bolonick, J. I. *J. Am. Chem. Soc.* **1996,** *118,* 10989.

[50] Lebrun, A.; Lavery, R. *Nucl. Acid. Res.* **1996,** *24,* 2260.

[51] Hummer, G.; Szabo, A. *Proc. Natl. Acad. Sci. USA* **2001,** *98,* 3658-3661.

[52] Jarzynski, C. *Phys. Rev. Lett.* **1997,** *78,* 2690-2693.

[53] Noy, A. *Appl. Phys. Lett.* **2004,** *85,* 4792-4794.

[54] Evans, E.; Williams, P. Dynamic Force Spectroscopy: I. Single Bonds. In *Physics of Bio-Molecules and Cells*, Vol. 75; Flyvbjerg, H.; Jlicher, F.; Ormos, P.; David, F., Eds.; Springer and EDP Sciences: Heidelberg, 2002.

[55] Strunz, T.; Oroszlan, K.; Schafer, R.; Guntherodt, H. J. *Proc. Natl. Acad. Sci. USA* **1999,** *96,* 11277-11282 SEP 28.

[56] Ratto, T. V.; Langry, K.; Rudd, R.; Balhorn, R.; McElfresh, M. *Biophys. J.* **2004,** *86,* 322A.

[57] Bustamante, C.; Marko, J. F.; Siggia, E. D.; Smith, S. *Science* **1994,** *265,* 1599-600.

[58] Brockwell, D. J.; Paci, E.; Zinober, R. C.; Beddard, G. S.; Olmsted, P. D.; Smith, D. A.; Perham, R. N.; Radford, S. E. *Nature Struct. Biol.* **2003,** *10,* 731-737.

[59] Fernandez, J. M.; Li, H. B. *Science* **2004,** *303,* 1674-1678.

[60] Tskhovrebova, L.; Trinick, J.; Sleep, J.; Simmons, R. *Nature* **1997,** *387,* 308-312.

[61] Smith, D. A.; Brockwell, D. J.; Zinober, R. C.; Blake, A. W.; Beddard, G. S.; Olmsted, P. D.; Radford, S. E. *Phil. Trans. Roy. Soc., Ser. A* **2003,** *361,* 713-728.

[62] Rief, M.; Oesterhelt, F.; Heymann, B.; Gaub, H. *Science* **1997,** *275,* 1295-1297.

[63] Prime, K. L.; Whitesides, G. M. *Science* **1991,** *252,* 1167 0036-8075.

[64] Oesterhelt, F.; Rief, M.; Gaub, H. E. *New J. Phys.* **1999,** *1,* 1-11.

[65] Friedsam, C.; Wehle, A. K.; Kuhner, F.; Gaub, H. E. *J. Phys. Cond. Matt.* **2003,** *15,* S1709-S1723.

[66] Williams, P. *Anal. Chim. Acta* **2003,** *479,* 107-115.

[67] Sulchek, T. A.; Friddle, R. W.; Noy, A. *Biophys. J.* **2005,** submitted.

[68] Miyatani, T.; Horii, M.; Rosa, A.; Fujihira, M.; Marti, O. *Appl. Phys. Lett.* **1997,** *71,* 2632-2634.

[69] Okabe, Y.; Furugori, M.; Tani, Y.; Akiba, U.; Fujihira, M. *Ultramicroscopy* **2000,** *82,* 203-212.

[70] Heinz, W. F.; Hoh, J. *Trends Biotech.* **1999,** *17,* 150 0167-7799.

[71] Noy, A.; Sanders, C. H.; Vezenov, D. V.; Wong, S. S.; Lieber, C. M. *Langmuir* **1998,** *14,* 1508-1511.

[72] Hinterdorfer, P.; Baumgartner, W.; Gruber, H. J.; Schilcher, K.; Schindler, H. *Proc. Natl. Acad. Sci. USA* **1996,** *93,* 3477-3481.

[73] Raab, A.; Han, W.; Badt, D.; Smith-Gill, S. J.; Lindsay, S. M.; Schindler, H.; Hinterdorfer, P. *Nature Biotech.* **1999,** *17,* 901-905.

[74] Gabai, R.; Segev, L.; Joselevich, E. *J. Am. Chem. Soc.* **2005,** *127,* 11390-11398.